DOI: 10.21062/mft.2025.067 http://www.journalmt.com

Strategy for Fabricating Tree-Like Branched Al-Al_2Cu Heterogeneous Nanostructures for Future Application in Battery Anodes

Elena Chochoľaková (0009-0002-6585-531X), Lucia Bajtošová (0000-0002-4746-9231), Nikoleta Štaffenová (0009-0006-9366-0666), Jan Hanuš (0000-0002-5825-8536), Peter Minárik (0000-0001-7034-5547), Miroslav Cieslar (0000-0002-2801-3810)
Charles University, Faculty of Mathematics and Physics, Ke Karlovu 3, 12116 Prague, Czech Republic.
E-mail: lucia.bajtosova@matfyz.cuni.cz

Tree-like branched Al-Al_2Cu heterogeneous nanostructures with a high surface area ratio were successfully fabricated using magnetron sputtering of Al matrix and Cu nanoparticles, followed by in situ annealing. The method enables precise control over the composition and morphology of the nanosized columnar Al_2Cu phase grown on the substrate and embedded in the Al matrix. The formation of Al_2Cu begins at the initial locations of sputtered Cu nanoparticles. Further annealing promotes their coalescence and coarsening. Orientation relationships examined in several Al_2Cu particles revealed a semi-coherency with the Al matrix. The high surface area and tunable composition highlight the potential of these nanostructures for advanced battery anodes, with tailored geometry achieved through controlled processing conditions.

Keywords: Al-Al_2Cu nanostructures, Magnetron sputtering, In situ TEM annealing

1 Introduction

Nanofabrication techniques have revolutionized material design by enabling precise control over microstructures and properties at the nanoscale [1, 2]. In battery electrodes, the geometry of the anode plays a critical role as it can facilitate the diffusion of ions, offering the possibility of faster charging batteries. The production of nanostructured anodes is widely utilized across various materials, including nanostructured lithium anodes [3] and lamella-nanostructured eutectics [4].

Aluminum-based eutectic composites are widely studied for their unique ability to balance strength and toughness, making them suitable for applications at ambient and elevated temperatures [5-7]. The intermetallic phases are particularly effective in Al-Si, Al-Cu, or Al-Cu-Si systems [8-12]. Eutectic Al-Cu composites exhibit a bimodal microstructure characterized by micrometer-sized dendrites embedded within a matrix of nano- or ultrafine-scale eutectics [10,13]. These dendrites are known to grow in specific crystallographic orientations relative to the matrix [14], modifying the properties of the composites and also contributing to their thermal and mechanical stability [15]. Moreover, Al-Al_2Cu composites are promising in electrochemical applications, particularly aluminum-based batteries. Water-based aluminum batteries are particularly appealing, as they are cheaper, safer, and less toxic than conventional lithium-ion batteries, which rely on flammable organic electrolytes [16,17].

However, the undesirable formation of oxide layers on the anodes from pure aluminum increases the internal resistance of the batteries and reduces their efficiency. At the same time, hydrogen gas generation during cycling decreases the size of the anode and the electrolyte volume, further limiting battery performance [18]. Also, dendrites formed on the anode during repeated charging cycles shorten battery life and increase the risk of failure. To overcome these drawbacks, the use of Al-Al_2Cu nanostructures as an anode material has been proposed [19]. An ordered lamellar nanostructure of alternating α-Al and intermetallic Al_2Cu lamellas produced via eutectic solidification exhibits exceptional Al stripping/plating stability because the more noble Al_2Cu lamellas serve as 2D nanopatterns to guide highly reversible Al stripping and plating.

The geometry of the anode plays a critical role. Further increase of the surface area between Al_2Cu and Al is desirable. It can be achieved by fabricating tree-like branched structures of Al_2Cu within the Al matrix. A simple way to prepare such nanostructures is to employ magnetron sputtering combined with gas aggregating sources [20, 21] instead of the eutectic reaction. The method offers flexibility in simultaneously depositing Cu nanoparticles and layers of Al. The relative deposition rates of the sputtered elements can be finely tuned, allowing for the controlled formation of heterogeneous structures of Cu nanoparticles immersed in the Al matrix or covered by Al layers.

Following the deposition, annealing should be performed to facilitate the diffusion of copper into the aluminum matrix, potentially leading to the formation of Al_2Cu-phase particles.

The primary aim of this work is to explore the potential of magnetron sputtering with the gas aggregating source in the design and fabrication of Al-Al_2Cu nanostructures suitable for future electrochemical applications. The tree-like branched Al-Al_2Cu heterogeneous nanostructures characterized by a high density of interconnected Al_2Cu particles inside the Al matrix with a high surface area ratio were prepared and analyzed.

2 Methods

The Al-Cu nanostructures were produced using a dual-chamber system. A primary gas aggregation cluster source (GAS) was employed to generate Cu nanoparticles (NPs). At the same time, an arrow-shaped secondary chamber was used to coat the Cu NPs with a thin Al film. This setup, which was previously utilized for sputtering Ni-Ti core-shell nanoparticles, is detailed by Hanus et al. [22]. The specimens were deposited on a photoresist-covered glass substrate. First, the pure Al layer was deposited for one minute. Subsequently, Al and Cu nanoparticles were sputtered for ten minutes, and this nanocomposite was again covered with a pure Al layer sputtered for one minute. The sputtering conditions were as follows: a pressure of 0.12 Pa, the Cu magnetron current of 316 mA at 316 V, and the Al magnetron current of 100 mA at 377 V. The schematical structure of the specimen is shown in Figure 1 a). After annealing, the composition can be further adjusted by depositing additional Al layers (Figure 1b).

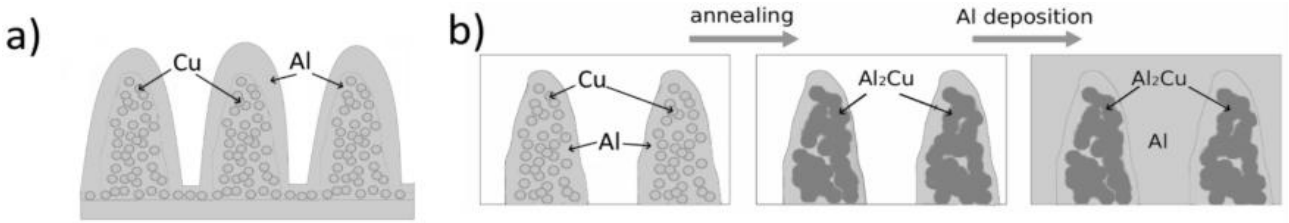

Fig. 1 *Schematics of the sputtering process: a) sputtering of an Al-(Al+Cu)-Al thin layer for transmission electron microscopy observations, and b) preparation of Al-Al_2Cu heterogeneous nanostructure*

Freestanding samples for transmission electron microscopy (TEM) were obtained by dissolving the photoresist substrate in acetone after fixing the film in TEM folding grids. The cross-sectional lamella was prepared using a focused ion beam in a Zeiss Auriga scanning electron microscope (SEM).

The specimens were characterized by a JEOL 2200FS TEM operated at 200 kV using TEM and scanning TEM (STEM) mode with bright field (BF) and high angle annular dark field (HAADF) detectors combined with energy-dispersive X-ray spectroscopy (EDX). The morphology of the resulting nanostructures was monitored in the scanning electron microscopy (SEM) mode using an in-lens secondary electron (SE) detector. Moreover, phase orientation maps using automated orientation phase mapping (ACOM-TEM) with an ASTAR software package and high-resolution TEM (HRTEM) images were captured. The specimens were annealed in situ in the same microscope using the Gatan heating holder.

3 Results

The initial characterization of the heterogeneous structure prepared by iteratively sputtering the pure Al and Al together with Cu nanoparticles in three consecutive layers is shown in Figure 2. The Al matrix embeds Cu NPs of the mean size of 15 nm (Fig. 2 a,b,e-h), forming a coarse surface with branched columns of various heights (Fig. 2 c). The separate face-centered cubic (fcc) Al and fcc Cu phases were confirmed by selected area electron diffraction (SAED) (Fig. 2d). A cross-sectional side view of the 30 nm thick Al film with a nanostructured columnar layer (Fig. 2i) enables the estimation of the total thickness (250 nm) and the maximal difference between the heights of columns (30 nm).

The composition of columns was estimated using two methods. First, an estimation was made from the number of Cu spheres with known radii in the 100 nm^3 region. Second, elemental quantification from EDS analysis of a 1x1 μm^2 large area was made. The image-based analysis yielded 20 % Cu and 80 % Al (at.%). However, this method may underestimate the Cu content due to the overlap of Cu nanoparticles. In contrast, EDS analysis yields approximately 30 % Cu and 70 % Al. Considering these factors, the average composition likely lies between these estimates. However, the versatility of the preparation method enables sensitive tailoring of the resulting composition by modifying the magnetron sputtering parameters, allowing a wider range of compositions and structures to be achieved.

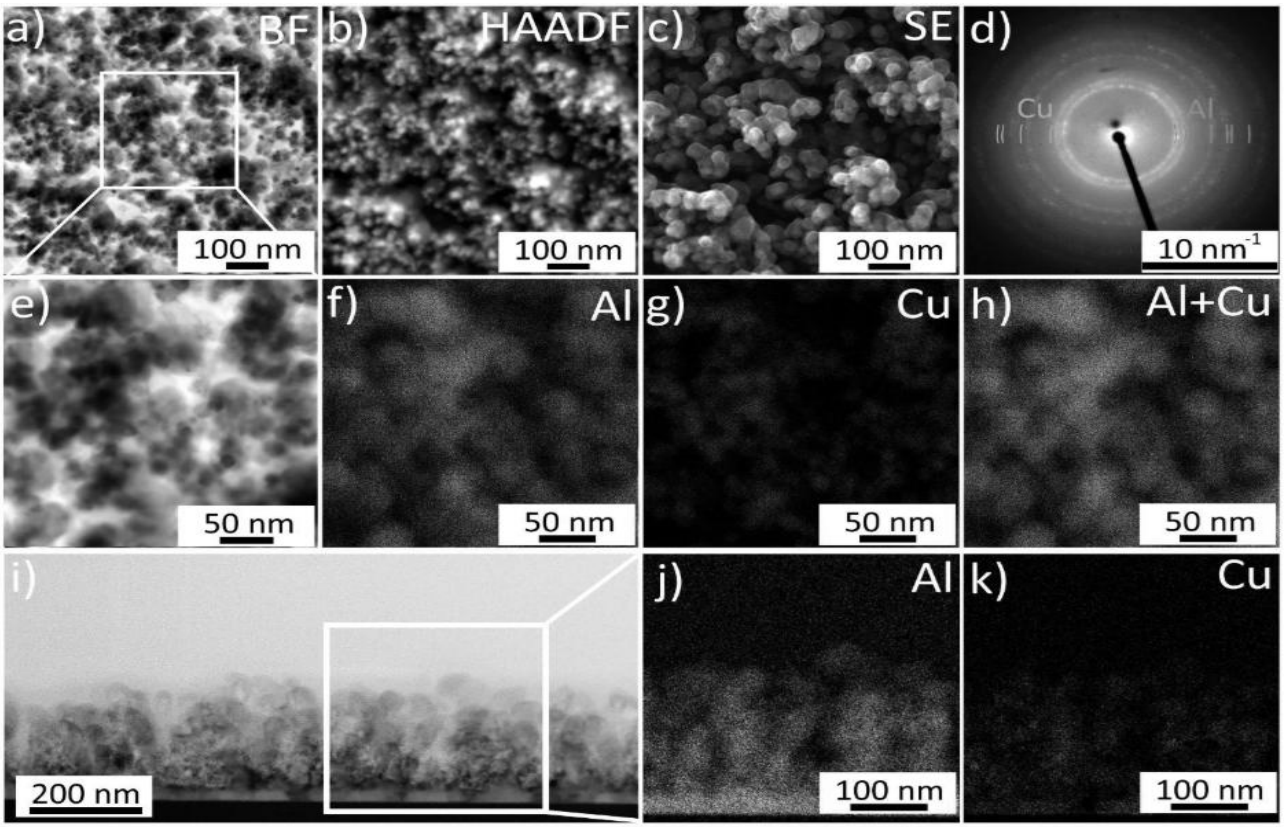

Fig. 2 *Initial state of the nanostructure; a) – c) plan-view, STEM images: a) bright field (BF) and b) high annular dark field (HAADF), c) secondary electrons detector (SE), d) selected area diffraction (SAED), e-h) detail of the plan-view with EDS maps: e) STEM BF, f) EDX Al map, g) EDS Cu map, h) EDS Al and Cu overlay, i-k) cross-section lamella: (i) HAADF and (j-k) EDS maps*

The specimen was then annealed in situ up to 350 °C in 50 °C steps, holding each temperature for 5 minutes. Figure 3 shows structural evolution during annealing. SE images (Fig. 3a–d) show no significant changes in the surface morphology throughout the entire temperature range. At 100 °C, no noticeable changes were observed in the shape of the Cu nanoparticles or the diffraction patterns (Fig. 3 f, j). Above 200 °C, the transformation of Cu nanoparticles is evident, as their sharp edges become diffuse and less distinct (Fig. 3 g). A low-intensity diffraction ring corresponding to (101) diffraction of tetragonal Al_2Cu (I4/mcm, lattice parameters 0.6063 nm and 0.4872 nm [23]) appears at this temperature (Fig. 3 k). This process is more pronounced during annealing at 350 °C (Fig 3 h). The diffraction pattern confirms a transformation of Al rings from the initially smooth ones into more distinct individual spots, indicating the coarsening of Al grains. New diffraction rings containing coarse spots corresponding to Al_2Cu became more evident. Among them, the one corresponding to (222)Al_2Cu is the most noticeable.

The Al_2Cu phase was localized in the nanocomposite by ACOM TEM mapping. A 500 × 500 nm² area was scanned with a pixel size of 2.5 nm². Virtual dark field (VDF) images were created using LiberTEM software [24], employing fluctuation electron microscopy (EM) analysis. The resulting images were matched with the HAADF images, as shown in Figure 4. The VDF was generated from the diffraction ring corresponding to the first Al_2Cu reflection, specifically from the (101) planes (inset in Figure 4). This method effectively highlights regions where they are the Al_2Cu particles suitably oriented ((101) planes in diffracting conditions). However, not all Al_2Cu areas can be detected; only those large enough to produce sufficient diffraction intensity relative to the surrounding matrix are visible. Al_2Cu in the form of small particles with radii slightly larger than the original Cu particles (15-25 nm) can be detected. Occasionally, larger Al_2Cu particles with radii up to 40 nm were observed. The highlighted Al_2Cu regions in VDF images overlap with Cu-rich regions in the thin areas visible in the HAADF maps.

EDS maps of the same area were acquired (Figure 4e-g), revealing Cu-rich regions. By comparing to the VDF image, Al_2Cu regions can be matched to the Cu-rich regions in the EDS image (Figure 4 c, d, g – blue circle and arrows). The composition of the Al_2Cu particle highlighted in Figure 4g (blue circle) can be quantified as 62% Al and 38% Cu, confirming a partial non-stoichiometry of the phase. Similar compositions were observed in other Cu-enriched regions of the map (Figure 4g indicated by blue arrows). This analysis further confirms the transformation of Cu nanoparticles into the Al_2Cu phase embedded in the Al matrix.

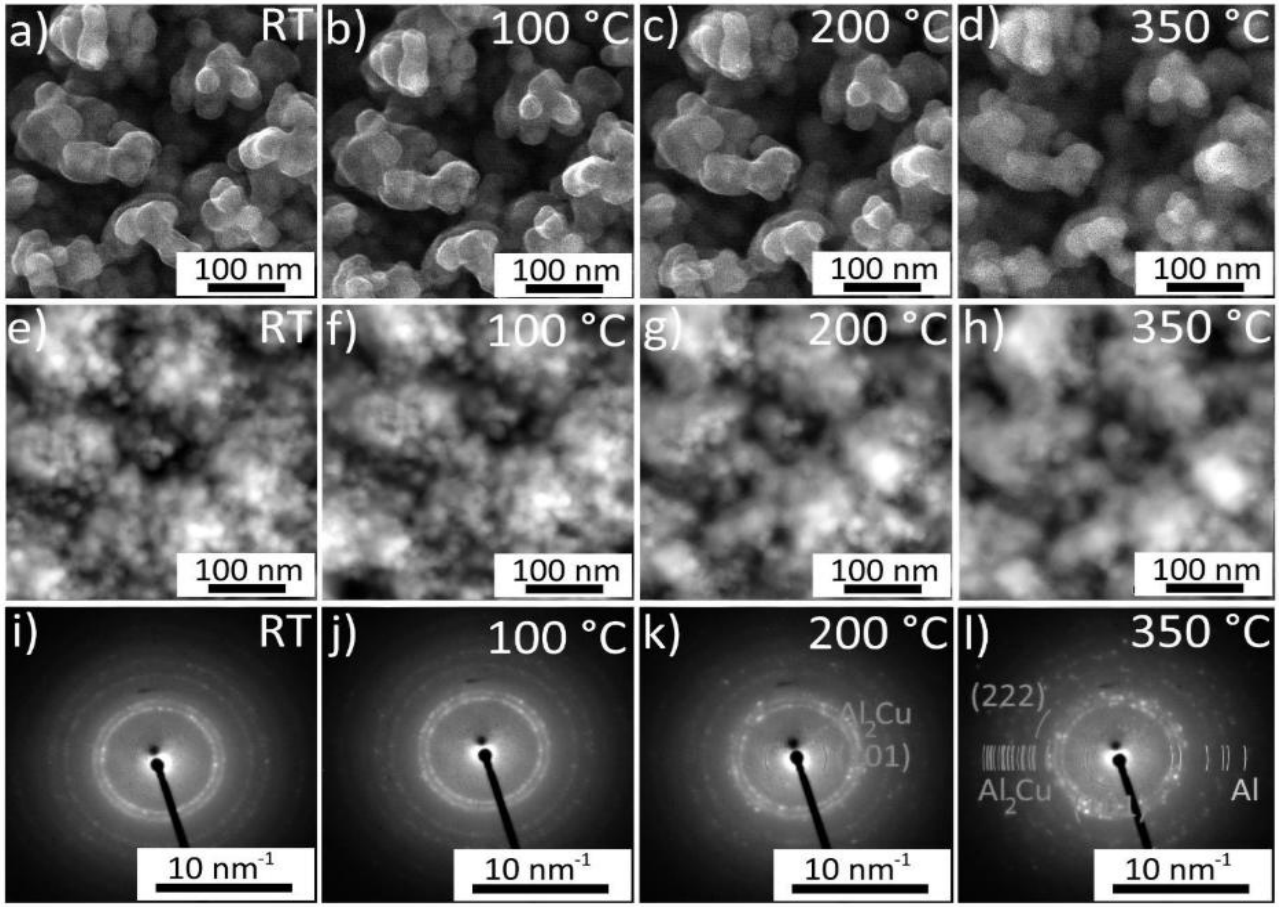

Fig. 3 *Annealing of the specimen from room temperature (RT) to 350 °C; Plan-view, a-d) SE images, e-h) HAADF images, i-l) SAED patterns*

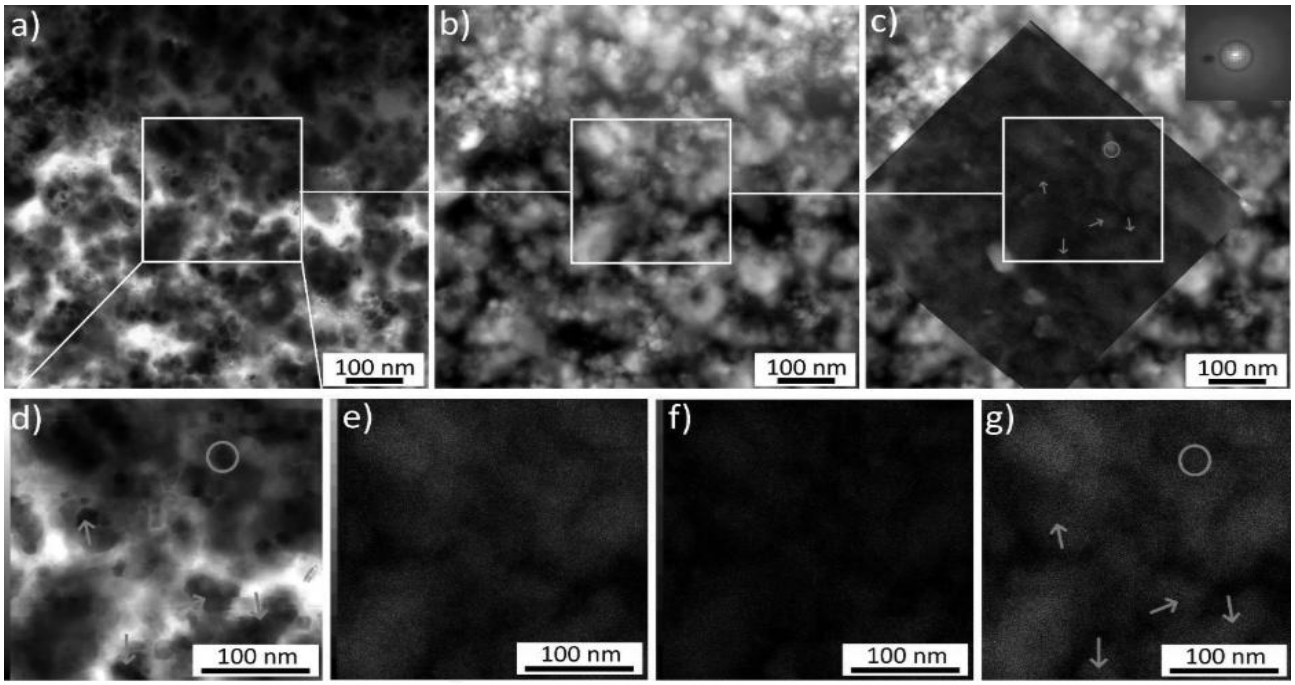

Fig. 4 *Specimen annealed to 350 °C: a) STEM BF, b) STEM HAADF, c) STEM HAADF overlapped with ACOM TEM virtual DF, where lighter coloring corresponds to higher intensity from the annular region associated with the reciprocal distance of (101) planes of Al_2Cu, highlighted in red in the diffraction pattern in the inset, d) STEM BF of an area inside the white square, e-g) EDS analysis of the same area e) Al map, f) Cu map, g) overlap of Al and Cu, parts with increased concentration of Cu are indicated by blue arrows*

Figure 5 shows an example of the HRTEM analysis of the interface between the Al matrix and the Cu-rich particles. Only the Al_2Cu phase was identified. The two interconnected particles with approximately 20 nm and 40 nm diameters are oriented along two different zone axes (Fig. 5 a,b, d,f). Figures 5c and 5e show the details of boundaries with the neighboring Al grains. For the larger particle, there is a high degree of coherency, with the following orientation relationship (OR): <110>Al ‖ <111>Al_2Cu and (1-11)Al ‖ (1-21)Al_2Cu. Additional parallel planes include (-1-10)Al ‖ (-110)Al_2Cu, (1-13)Al ‖ (0-11)Al_2Cu, (001)Al ‖ (-1-12)Al_2Cu. The interface plane is close to (1-11)Al ‖ (1-21)Al_2Cu. For the smaller particle, the boundary OR is characterized by (1-11)Al ‖ (001)Al_2Cu, with <110>Al being approximately parallel to ⟨110⟩Al_2Cu.

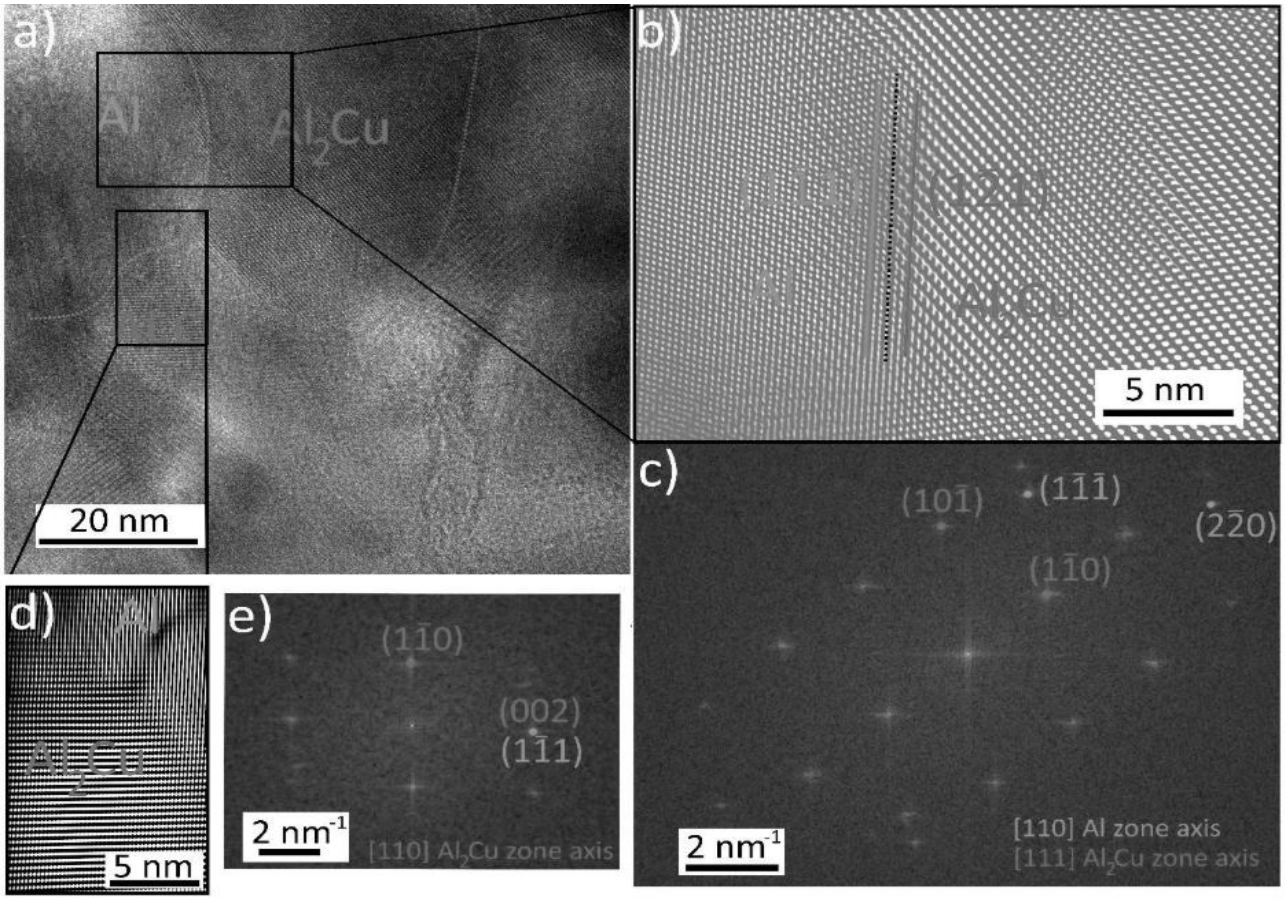

Fig. 5 *HRTEM images of the specimen annealed to 350 °C, a) HRTEM, b,d) FFT filtered image of details of boundaries between Al and Al phases, and c, e) corresponding FFT patterns used to create filtered images, with diffraction spots marked in color (blue Al, green Al_2Cu) in the FFT patterns*

4 Discussion

Figure 6 illustrates the transformation process of Cu NPs. Small (14 - 15 nm large) particles at RT slowly grow at 200 °C and transform into 28 - 36 nm large particles at 250 - 350 °C. Considering diffusion lengths calculated from corresponding volume diffusion coefficients (Figure 7), the diffusion length of Cu in Al after 300 seconds is 10 nm at 200 °C, 50 nm at 250 °C, and 620 nm at 350 °C. Given the length scale of the specimen, annealing at 350 °C is sufficient for the Cu atoms to reach all parts of the specimen. The diffusion coefficient of Al in Cu is significantly lower, resulting in negligible diffusion lengths at the same temperatures.

The size of Al_2Cu particles formed from Cu particles can be calculated based on the conservation of mass and the difference in densities between Cu (8.96 g/cm^3) and Al_2Cu (4.0 g/cm^3). The initial Cu particle volume and mass were used to determine the equivalent Al_2Cu particle volume and diameter, assuming a spherical geometry. The Cu particles with diameters of 10 nm, 15 nm, and 20 nm can grow into Al_2Cu particles with sizes 12.5 nm, 19.4 nm, and 25.5 nm. Using this estimation, it becomes evident that several Cu nanoparticles need coalescence to form Al_2Cu particles as large as 36 nm in diameter. For example, three 15 nm large (Fig 6 a) blue circle) Cu nanoparticles would form 28 nm large Al_2Cu nanoparticle (Fig 6 g) blue circle) D). The minor individual growth with loss of diffraction contrast observed at 200 °C can contribute to the start of the phase transformation, while the more noticeable growth at 250 - 350 °C results from the coalescence of particles.

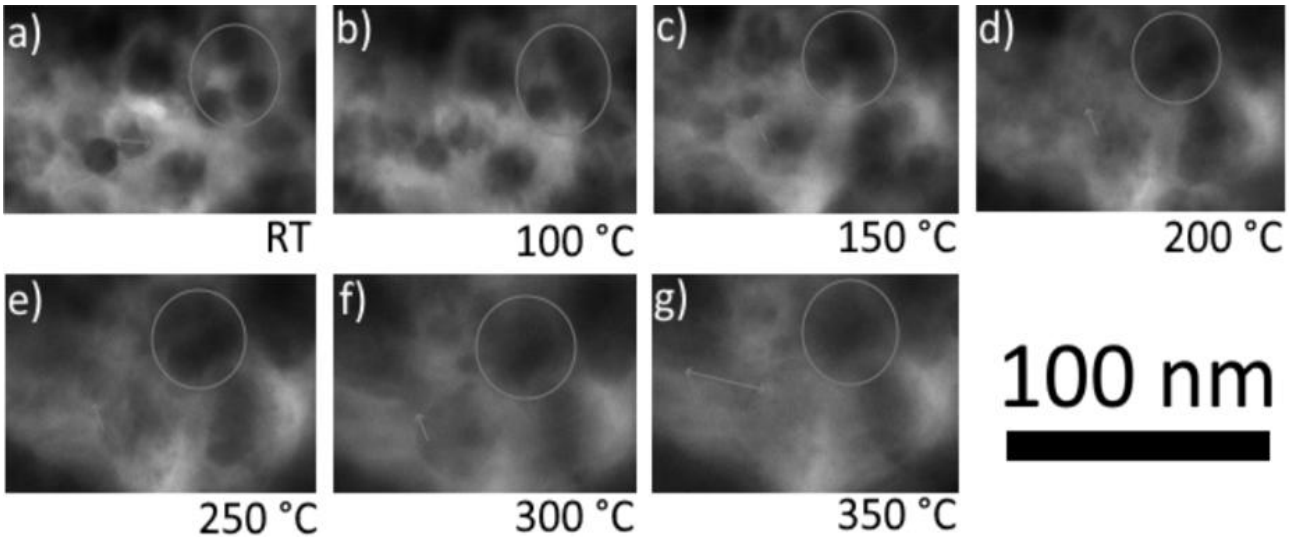

Fig. 6 *STEM BF analysis of the transformation of Cu nanoparticles during in situ annealing*

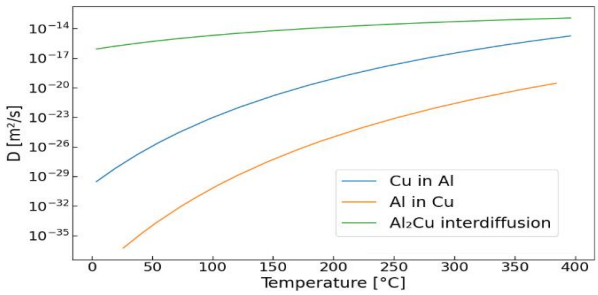

Fig. 7 *Interdiffusion coefficients of Al in Cu, Cu in Al, and combined interdiffusion coefficient of Al and Cu in Al_2Cu [25, 26]*

The system of Cu nanoparticles embedded in the Al matrix exhibits similarities to an interface-controlled Al-Cu reaction. Al_2Cu is widely recognized as the initial nucleation phase at Al-Cu interfaces, driven by localized diffusion phenomena. The solubility of Al in Cu is relatively high, reaching 19.7 at.% within the 400–500 °C temperature and corresponds to conditions near the eutectic temperature (548 °C). Conversely, the solubility of Cu in Al is markedly lower, with a maximum of 2.48 at.% in the same temperature range [25, 26]. At temperatures below 200 °C, the solubility of Cu in Al decreases to less than 0.1 at.% [27]. Due to this substantial difference in solubility limits, with Cu being far less soluble in Al than Al in Cu, the Al(Cu) solid solution is expected to reach saturation first. This saturation facilitates the nucleation of Al_2Cu as the primary precipitate phase. Moreover, Al_2Cu as the primary precipitate phase can also be predicted by the effective heat of formation (EHF) model developed by Pretorius et al. [28, 29] for phase formation in diffusion-controlled systems. Among the possible phases, Al_2Cu exhibits the most negative effective heat of formation, making it the most thermodynamically favorable phase to form initially in the diffusion zone [25].

These predictions align with experimental observations of Al-Cu interfaces in multilayered thin films [25, 30, 31]. For instance, in Al-Cu multilayered films over 100 μm thick, intermetallic phases such as Al_4Cu_9, AlCu, and Al_2Cu were observed to form within the temperature range of 400–500 °C. Notably, under these conditions, the Al_2Cu phase exhibited a significant layer thickness exceeding 2 μm. In ultrathin multilayer films, such as $(Al/Cu)_{50}$ systems with alternating Al (22 nm) and Cu (37 nm) layers, Al_2Cu forms at temperatures as low as 100 °C. The Al_4Cu_9 phase also appears after approximately 8 minutes of annealing at the same temperature. These findings highlight the importance of alloy composition and the annealing dynamics in determining the resulting phases.

In our specific case, the Cu/Al ratio was sufficiently low to prevent the formation of the Al_4Cu_9 phase, favoring the nucleation and growth of Al_2Cu instead. The growth process was directly linked to the original locations of Cu particles. At lower temperatures, Al_2Cu consistently formed in the positions close to where the Cu particles were initially deposited. As Cu atoms diffuse into the surrounding Al matrix, the boundary between Cu and Al moves inward, causing the shrinkage of the Cu particle. The layer of Al_2Cu starts to form on the boundary. Since the interdiffusion coefficient of Al and Cu in Al_2Cu at 200 °C is 105 times higher than the diffusion coefficients of Cu in Al and Al in Cu (Figure 7), the phase can grow in both directions and fully encompass the entire particle.

5 Conclusions

Heterogeneous Al-Al_2Cu nanostructures containing Al_2Cu nanocolumns within the Al matrix were successfully fabricated using magnetron sputtering with gas aggregation cluster source and in situ annealing. Magnetron sputtering proved to be a versatile and

controllable method for synthesizing Al-Al_2Cu nanostructures, offering control over the material composition and morphology.

- The formation of the Al_2Cu phase begins at 200 °C, and this phase remains the sole one formed within the temperature range 200 °C – 350 °C.
- The Al_2Cu phase forms as nanoscale particles in the exact locations of the originally sputtered Cu nanoparticles.
- Most of the Cu nanoparticles transform to the Al_2Cu phase at 200 °C. Further annealing leads to their coalescence and coarsening.
- Orientation relationships retain a high degree of coherency with the Al matrix and the specific orientation relationships with the matrix, such as (1-11)Al || (1-21)Al_2Cu.

Acknowledgement

The authors would like to thank the support from Grant Agency of Charles University under the project 280223.

References

[1] SATYA, H., GUPTA, S., et al. (2023). Nanofabrication of metals and their compounds for effective medicinal and environmental applications (a review). In: *Russian Journal of General Chemistry*, 93, 635–665. https://doi.org/10.1134/S1070363223030209

[2] CHEN, Y. (2015). Nanofabrication by electron beam lithography and its applications: A review. In: *Microelectronic Engineering*, 135, 57–72. https://doi.org/10.1016/j.mee.2015.02.042

[3] ARMSTRONG, M. J., O'DWYER, C., MACKLIN, W. J., et al. (2014). Evaluating the performance of nanostructured materials as lithium-ion battery electrodes. In: *Nano Research*, 7, 1–62. https://doi.org/10.1007/s12274-013-0375-x

[4] WANG, S. B., RAN, Q., YAO, R. Q., et al. (2020). Lamella-nanostructured eutectic zinc–aluminum alloys as reversible and dendrite-free anodes for aqueous rechargeable batteries. In: *Nature Communications*, 11, 1634. https://doi.org/10.1038/s41467-020-15478-4

[5] PARK, J. M., KIM, K. B., KIM, D. H., MATTERN, N., LI, R., LIU, G., & ECKERT, J. (2010). Multi-phase Al-based ultrafine composite with multi-scale microstructure. In: *Intermetallics*, 18(10), 1829–1833. https://doi.org/10.1016/j.intermet.2010.02.042

[6] TIWARY, C. S., KASHYAP, S., KIM, D. H., & CHATTOPADHYAY, K. (2015). Al-based ultra-fine eutectic with high room temperature plasticity and elevated temperature strength. In: *Materials Science and Engineering: A*, 639, 359–369. https://doi.org/10.1016/j.msea.2015.05.024

[7] CZERWINSKI, F., ANIOLEK, M., & LI, J. (2022). Strengthening retention and structural stability of the Al-Al_3Ni eutectic at high temperatures. In: *Scripta Materialia*, 214, 114679. https://doi.org/10.1016/j.scriptamat.2022.114679

[8] LI, X. P., WANG, X. J., SAUNDERS, M., SUVOROVA, A., ZHANG, L. C., LIU, Y. J., FANG, M. H., HUANG, Z. H., & SERCOMBE, T. B. (2015). A selective laser melting and solution heat treatment refined Al–12Si alloy with a controllable ultrafine eutectic microstructure and 25% tensile ductility. In: *Acta Materialia*, 95, 74–82. https://doi.org/10.1016/j.actamat.2015.05.017

[9] ARAVIND, M., YU, P., YAU, M. Y., & NG, D. H. L. (2004). Formation of Al_2Cu and AlCu intermetallics in Al(Cu) alloy matrix composites by reaction sintering. In: *Materials Science and Engineering: A*, 380(1–2), 384–393. https://doi.org/10.1016/j.msea.2004.04.013

[10] PARK, J. M., MATTERN, N., KÜHN, U., ECKERT, J., KIM, K. B., KIM, W. T., CHATTOPADHYAY, K., & KIM, D. H. (2009). High-strength bulk Al-based bimodal ultrafine eutectic composite with enhanced plasticity. In: *Journal of Materials Research*, 24, 2605–2609. https://doi.org/10.1557/jmr.2009.0297

[11] VLACH, T., CAIS, J., MAMOŇ, F., & MAREŠ, J. (2024). The effect of the solution annealing temperature in the hardening process on the properties of Al–Si–Cu alloys. *Manufacturing Technology*, 24(1), 141–147. https://doi.org/10.21062/mft.2024.011

[12] SÝKOROVÁ, M., BOLIBRUCHOVÁ, D., BRŮNA, M., & CHALUPOVÁ, M. (2024). Effect of solubility of alloying elements on selected properties and on the structure of AlSi5Cu2Mg. *Manufacturing Technology*, 24(5), 817–826. https://doi.org/10.21062/mft.2024.078

[13] KIM, J. T., LEE, S. W., HONG, S. H., PARK, H. J., PARK, J. Y., LEE, N., SEO, Y., WANG, W. M., PARK, J. M., & KIM, K. B. (2016). Understanding the relationship between microstructure and mechanical properties of Al–Cu–Si ultrafine eutectic composites.

In: *Materials & Design*, 92, 1038–1045. https://doi.org/10.1016/j.matdes.2015.12.080

[14] GAO, K., LI, S. M., XU, L., & FU, H. Z. (2014). Effect of sample size on intermetallic Al_2Cu microstructure and orientation evolution during directional solidification. In: *Journal of Crystal Growth*, 394, 89–96. https://doi.org/10.1016/j.jcrysgro.2014.02.023

[15] ZHOU, Q., HUA, D. P., DU, Y., REN, Y., KUANG, W. W., XIA, Q. S., & BHARDWAJ, V. (2019). Atomistic study of atomic structures and dislocation nucleation at Al/Al_2Cu interfaces. In: *International Journal of Plasticity*, 120, 115–126. https://doi.org/10.1016/j.ijplas.2019.04.014

[16] YAN, C., et al. (2020). Architecting a stable high-energy aqueous Al-ion battery. In: *Journal of the American Chemical Society*, 142(36), 15295–15304. https://doi.org/10.1021/jacs.0c05054

[17] JIA, B. E., et al. (2022). Rechargeable aqueous aluminum-ion battery: Progress and outlook. In: *Small*, 18(43), 2107773. https://doi.org/10.1002/smll.202107773

[18] PAN, W., WANG, Y., ZHANG, Y., KWOK, H. Y. H., WU, M., ZHAO, X., & LEUNG, D. Y. C. (2019). A low-cost and dendrite-free rechargeable aluminium-ion battery with superior performance. In: *Journal of Materials Chemistry A*. https://doi.org/10.1039/c9ta05207k

[19] RAN, Q., SHI, H., MENG, H., ZENG, S.-P., WAN, W.-B., ZHANG, W., WEN, Z., LANG, X.-Y., & JIANG, Q. (2022). Aluminum-copper alloy anode materials for high-energy aqueous aluminum batteries. In: *Nature Communications*, 13, 576. https://doi.org/10.1038/s41467-022-28238-3

[20] NIKITIN, D., HANUŠ, J., ALI-OGLY, S., POLONSKYI, O., DREWES, J., FAUPEL, F., BIEDERMAN, H., & CHOUKOUROV, A. (2019). The evolution of Ag nanoparticles inside a gas aggregation cluster source. In: *Plasma Processes and Polymers*, 16(7), 1900079. https://doi.org/10.1002/ppap.201900079

[21] KROBOTOVÁ, A., BAKALOVÁ, T., KRAFKA, M., MRÓZEK, M., SVOBODOVÁ, L., KEJZLAR, P., & TOMKOVÁ, B. (2025). Surface treatment of nylon filters with thin layers of Ti, Cu, and Zr metals and AgCu alloys using PVD magnetron sputtering technology. *Manufacturing Technology*, 25(3), 348–356. https://doi.org/10.21062/mft.2025.045

[22] HANUŠ, J., VAIDULYCH, M., KYLIÁN, O., CHOUKOUROV, A., KOUSAL, J., KHALAKHAN, I., CIESLAR, M., SOLAŘ, P., & BIEDERMAN, H. (2017). Fabrication of Ni@Ti core–shell nanoparticles by modified gas aggregation source. In: *Journal of Physics D: Applied Physics*, 50(47), 475307. https://doi.org/10.1088/1361-6463/aa8f25

[23] DONG, X., YANG, S., LI, N., ZHONG, H., WANG, X. Y., & DONG, H. (2024). The evolution and dissolution mechanism of θ-Al_2Cu phase and the analysis of precipitation of a novel AlCu phase during elevated aging. In: *Materials Characterization*, 217, 114454. https://doi.org/10.1016/j.matchar.2024.114454

[24] LIBERTEM DEVELOPMENT TEAM. (2024). LiberTEM (Version 0.14.1) [Software]. In: *Zenodo*. https://doi.org/10.5281/zenodo.12168380

[25] GERSHINSKII, A. E., FOMIN, B. I., CHEREPOV, E. I., & EDELMAN, F. L. (1977). Investigation of diffusion in the Cu-Al thin film system. In: *Thin Solid Films*, 42(3), 269–275. https://doi.org/10.1016/0040-6090(77)90246-3

[26] MOISEENKO, E. T., YUMASHEV, V. V., ALTUNIN, R. R., SOLOVYOV, L. A., VOLOCHAEV, M. N., BELOUSOV, O. V., & ZHARKOV, S. M. (2023). Thermokinetic study of intermetallic phase formation in an Al/Cu multilayer thin film system. In: *Materialia*, 28, 101747. https://doi.org/10.1016/j.mtla.2023.101747

[27] AARON, H. B., & AARONSON, H. I. (1968). Growth of grain boundary precipitates in Al–4% Cu by interfacial diffusion. In: *Acta Metallurgica*, 16(6), 789–798.

[28] PRETORIUS, R., VREDENBERG, A. M., SARIS, F. W., & DE REUS, R. (1991). In: *Journal of Applied Physics*, 70, 3636.

[29] PRETORIUS, R., MARAIS, T. K., & THERON, C. C. (1993). In: *Materials Science Reports*, 10, 1.

[30] GUO, Y., LIU, G., JIN, H., SHI, Z., & QIAO, G. (2011). Intermetallic phase formation in diffusion-bonded Cu/Al laminates. In: *Journal of Materials Science*, 46(7), 2467–2473. https://doi.org/10.1007/s10853-010-5093-0

[31] RASHKOVA, B., FALLER, M., PIPPAN, R., & DEHM, G. (2014). Growth mechanism of Al_2Cu precipitates during in situ TEM heating of a HPT deformed Al–3 wt.% Cu alloy. In: *Journal of Alloys and Compounds*, 600, 43–50. https://doi.org/10.1016/j.jallcom.2014.02.090